Isotropic magnetoelectric effect in $Tb_{1-x}Gd_xMn_2O_5$ studied by resonant x-ray scattering

Y. Ishii,[1,*] Y. Murakoshi,[2] N. Sato,[2] Y. Noda,[3] T. Honda,[4] H. Nakao,[1] Y. Murakami,[1] and H. Kimura[2,3]

[1]*Condensed Matter Research Center and Photon Factory, Institute of Materials Structure Science (IMSS), High Energy Accelerator Research Organization (KEK), Tsukuba, Ibaraki 305-0801, Japan*

[2]*Department of Physics, Tohoku University, Aoba, Sendai 980-8578, Japan*

[3]*Institute of Multidisciplinary Research for Advanced Materials, Tohoku University, Aoba Sendai 980-8577, Japan*

[4]*Neutron Science Division, Institute of Materials Structure Science, High Energy Accelerator Research Organization (KEK), Tsukuba, Ibaraki 305-0801, Japan*

(Received 5 June 2019; published 12 September 2019)

A new type of magnetoelectric (ME) effect was discovered in $Tb_{1-x}Gd_xMn_2O_5$ in which Gd ions are substituted into $TbMn_2O_5$. The substitution of Gd ions increased to $x = 0.5$ was found to completely suppress increases in electric polarization below $T \sim 14$ K, which is clearly observed in $TbMn_2O_5$. The electric polarization of $Tb_{0.5}Gd_{0.5}Mn_2O_5$ reappears below $T \sim 14$ K in response to an external magnetic field applied along each crystallographic axis. This isotropic ME effect is in distinction from those exhibited by the RMn_2O_5 family and by other multiferroic compounds. Resonant x-ray scattering was used to investigate the mechanism of the ME effect, and the data clearly demonstrate that this phenomenon can be attributed to competition between two different magnetic orderings. Furthermore, the magnetic-field dependence of the resonant intensity around the O K edge implies that charge transfer between O and Mn ions microscopically contributes to the ME effects. These findings indicate potential new applications for multiferroic materials.

DOI: 10.1103/PhysRevB.100.104416

I. INTRODUCTION

Multiferroics, which have more than one ferroic order parameter, have been under the focus of intensive research for several decades. Many multiferroic materials, such as $TbMnO_3$ and $MnWO_4$, exhibit magnetoelectric (ME) effect in which an external magnetic (electric) field leads to significant changes in dielectric (magnetic) properties of these compounds [1,2]. RMn_2O_5 (R = rare-earth) compounds have attracted much attention since they show various ME effects depending on the type of rare-earth ions. Examples of these ME effects include 180° and 90° rotation of electric polarization in response to a magnetic field applied along the a axis in $TbMn_2O_5$ and the c axis in $TmMn_2O_5$, respectively [3,4]. It is known for RMn_2O_5 compounds that a colossal ME effect appears when a magnetic field is applied along the direction of the rare-earth magnetic moment [5]. Magnetic ordering in various RMn_2O_5 compounds has been observed using techniques, such as neutron and x-ray scatterings, which have revealed Mn^{4+} and Mn^{3+} zigzag antiferromagnetic chain on the ab plane and/or Mn^{4+} cycloidal spin chain along the c axis in these materials [6–12]. Such complex magnetic ordering is believed to be responsible for the various ME effects and dielectric properties of these materials as a result of the break of inversion symmetry via exchange striction and/or inverse Dzyaloshinskii-Moriya effects [4,8,13–15].

Here, we investigated the dielectric and magnetic properties of $Tb_{1-x}Gd_xMn_2O_5$, synthesized by substituting Gd ions into $TbMn_2O_5$. Since $TbMn_2O_5$ and $GdMn_2O_5$ exhibit different magnetic ordering and dielectric properties [9,10,16], we expected that $Tb_{1-x}Gd_xMn_2O_5$ compounds might show new types of ME effects not seen before in the RMn_2O_5 family as a result of competition between the two different magnetic orderings. Figure 1 shows the dielectric and magnetic phase diagram for $Tb_{1-x}Gd_xMn_2O_5$ compounds, plotted as a function of Gd concentration x, based on data obtained in the present paper. The dielectric properties and magnetic ordering in $TbMn_2O_5$ and $GdMn_2O_5$ have been reported in the previous publications [9,10,16].

In the case of $TbMn_2O_5$, an incommensurate magnetic (ICM) ordering first appears at $T \sim 42$ K with the magnetic propagation vector $\mathbf{q}^1_{\mathrm{ICM}} = (1/2 + \delta_x, 0, 1/4 + \delta_z)$. The electric polarization along the b axis concomitantly appears at $T \sim 40$ K with a commensurate magnetic (CM) ordering with $\mathbf{q}^1_{\mathrm{CM}} = (1/2, 0, 1/4)$ [see also Fig. 2(a)]. This phase is denoted as FE1 in Fig. 1. The electric polarization decreases at $T \sim 25$ K (in the FE2 phase) as the magnetic ordering changes to an ICM ordering with $\mathbf{q}^1_{\mathrm{ICM}'} = (1/2 + \delta'_x, 0, 1/4 + \delta'_z)$ and the spontaneous magnetic ordering of Tb ions occurs. With further decreases in temperature, the electric polarization increases again below $T \sim 14$ K (in the FE3 phase) as a result of increases in the amplitude of Tb magnetic moments [17]. A colossal ME effect is also observed in that an external magnetic field applied along the a axis in the FE3 phase results in a flipping of the electric polarization [3].

Meanwhile, $GdMn_2O_5$ has relatively large electric polarization below $T \sim 36$ K as shown in Fig. 2(e) in which the magnetic moments of Mn ions align with the $\mathbf{q}^2_{\mathrm{CM}} = (1/2, 0, 0)$. Herein, we refer to this phase as the FE4 phase. The spontaneous magnetic ordering of Gd ions occurs at $T \sim 13$ K [9,10] and appears to be only minimally associated

*ishiiy@post.kek.jp

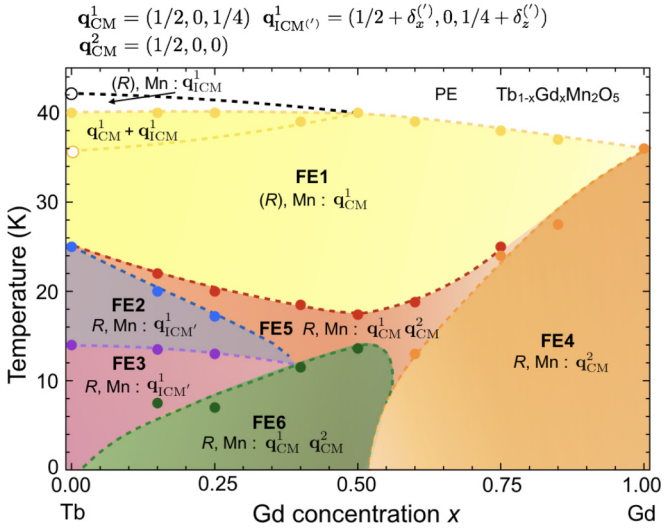

FIG. 1. Dielectric and magnetic phase diagram plotted as a function of Gd concentration x. Filled circles represent the data obtained from dielectric measurements in the present paper, whereas open circles indicate magnetic transition temperatures acquired in a previous neutron-scattering experiment [16]. Magnetic phases were estimated based on the present and previous experiments, where $\mathbf{q}^1_{CM} = (1/2, 0, 1/4)$, $\mathbf{q}^1_{ICM^{(\prime)}} = (1/2 + \delta^{(\prime)}_x, 0, 1/4 + \delta^{(\prime)}_z)$, and $\mathbf{q}^2_{CM} = (1/2, 0, 0)$. (R) represents rare-earth magnetic ordering induced by the moments of Mn ions.

with the electric polarization. Applying a magnetic field to $GdMn_2O_5$ results in minor changes in the electric polarization [18]. Thus, $TbMn_2O_5$ and $GdMn_2O_5$ exhibit varying dielectric properties due to their different magnetic orderings.

In the present study of $Tb_{1-x}Gd_xMn_2O_5$, an isotropic ME effect was discovered in the case of $Tb_{0.5}Gd_{0.5}Mn_2O_5$ where the electric polarization drastically increases in response to a magnetic field applied along each crystallographic axis. We performed resonant x-ray scattering (RXS), which clearly showed that this ME effect is associated with two different magnetic orderings. In addition, the effect of the magnetic field on the intensity at the O K edge suggests that charge transfer between O and Mn ions microscopically promotes the ME effect.

II. EXPERIMENTAL DETAILS

Single crystals of $Tb_{1-x}Gd_xMn_2O_5$ ($x = 0.00$, 0.15, 0.25, 0.40, 0.50, 0.60, 0.75, 0.85, or 1.00) were grown by the PbO-PbF_2 flux method [19]. Figure 3 plots lattice constants as functions of Gd concentration x, based on data from x-ray single-crystal structural analyses. These lattice parameters increase with increasing Gd concentration since the radius of the Gd^{3+} ion is larger than that of the Tb^{3+} ion. In addition, we confirmed that our samples were single crystals by x-ray structure analyses. Dielectric measurements were performed using a LCR meter and an electrometer with a commercial magnetometer at the High Energy Accelerator Research Organization (KEK).

RXS experiments were also performed around Mn $L_{II,III}$, O K, Gd, Tb L_{III}, and Gd and Tb M_V edges at BL-3A, BL-4C, BL-16A, and BL-19B [20,21] at the Photon Factory, KEK, Japan, employing π-polarized incident x rays. Note that, since a polarization analysis was not performed, π-σ' and π-π' processes both contributed to the scattering intensities in these measurements.

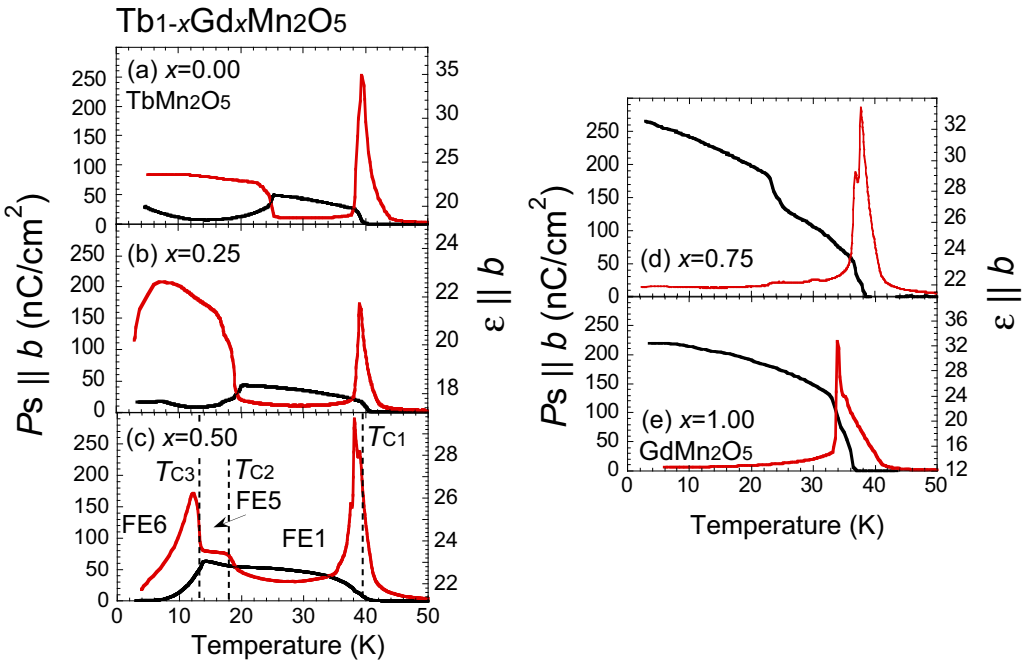

FIG. 2. Temperature dependence of electric polarization (black line) and dielectric constant (red line) along the b axis for compounds for which $x = 0.00$, 0.25, 0.50, 0.75, and 1.00.

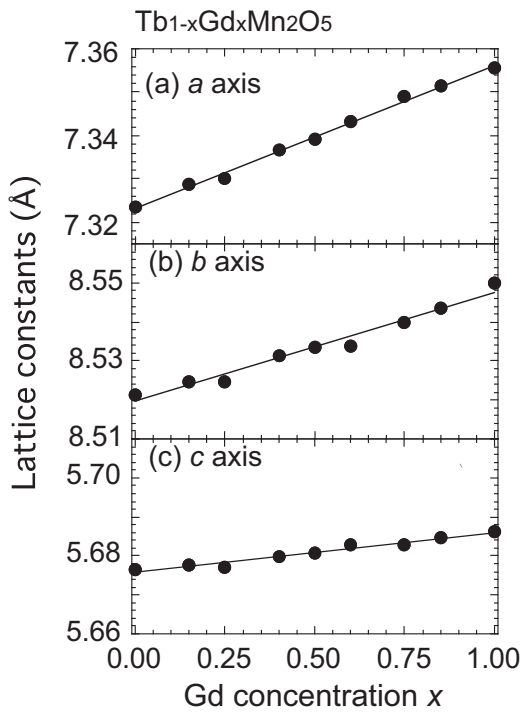

FIG. 3. Lattice constants at room temperature as a function of Gd concentration x.

III. RESULTS AND DISCUSSION

A. Dielectric measurements

Figure 2 shows temperature dependence of the electric polarization obtained from pyroelectric current measurement and the dielectric constant at a frequency of 10 kHz for $Tb_{1-x}Gd_xMn_2O_5$ ($x = 0.00$, 0.25, 0.50, 0.75, and 1.00). The electric polarization in $TbMn_2O_5$ increases again below $T \sim 14$ K. The extent of this increase is suppressed as the Gd concentration increases in the region of $x \leqslant 0.5$. In the case of $Tb_{0.5}Gd_{0.5}Mn_2O_5$, the electric polarization first appears at $T = T_{C1} \sim 40$ K as shown in Fig. 2(c), and this ferroelectric phase corresponds to the FE1 phase. A second dielectric transition occurs at $T = T_{C2} \sim 18$ K at which point the FE1 phase transitions to a different ferroelectric phase termed the FE5 phase as shown in Figs. 1 and 2(c). With further decreases in temperature, the electric polarization disappears at $T = T_{C3} \sim 14$ K at which point the FE6 phase appears. Dielectric constant shows a sharp anomaly at each phase-transition temperature, which suggests that each dielectric phase is a single phase. For the compounds with x more than 0.5, the FE4 phase appears with a large electric polarization. Based on these dielectric measurements, we obtained a dielectric phase diagram for $Tb_{1-x}Gd_xMn_2O_5$ as shown in Fig. 1.

We measured the ME effect in $Tb_{0.5}Gd_{0.5}Mn_2O_5$. Figures 4(a)–4(f) show temperature dependence of the electric polarization and the dielectric constant at various magnetic-field strengths. Below T_{C3} (in the FE6 phase), the electric polarization appears in response to an external magnetic field. It is noted that this colossal ME effect results from the application of an external magnetic field along each crystallographic axis, although the magnitude of the magnetic field leading to the ME effect varies slightly depending on the magnetic-field direction. This isotropic ME effect is in contrast to those in other RMn_2O_5 compounds and other multiferroic materials for which it is required to apply a magnetic field along a particular crystallographic axis to induce colossal ME effects. Hence, the finding of this isotropic ME effect points

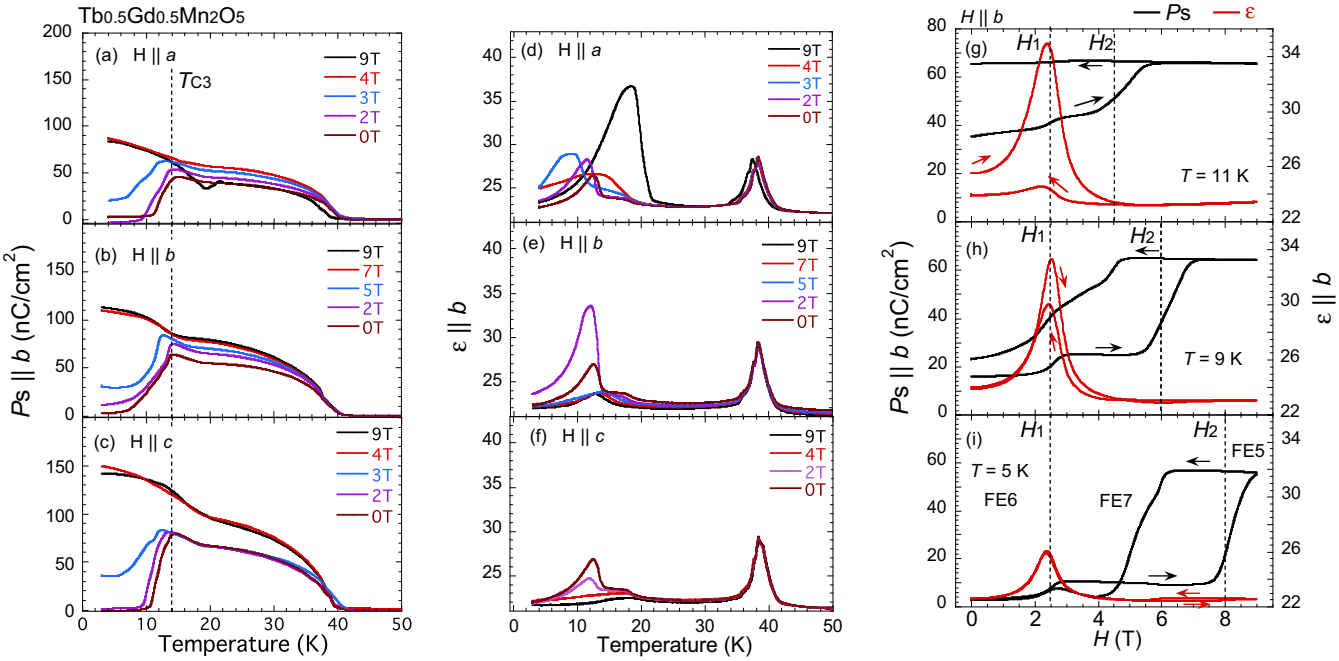

FIG. 4. Temperature profiles for [(a)–(c)] electric polarization and [(d)–(f)] the dielectric constant in $Tb_{0.5}Gd_{0.5}Mn_2O_5$ at various magnetic-field strengths along the a, b, and c axes. Magnetic-field ($H \parallel b$ axis) dependence of electric polarization (black line) and dielectric constant (red line) at (g) $T = 11$ K, (h) $T = 9$ K, and (i) $T = 5$ K. The arrows represent the magnetic-field sweep direction.

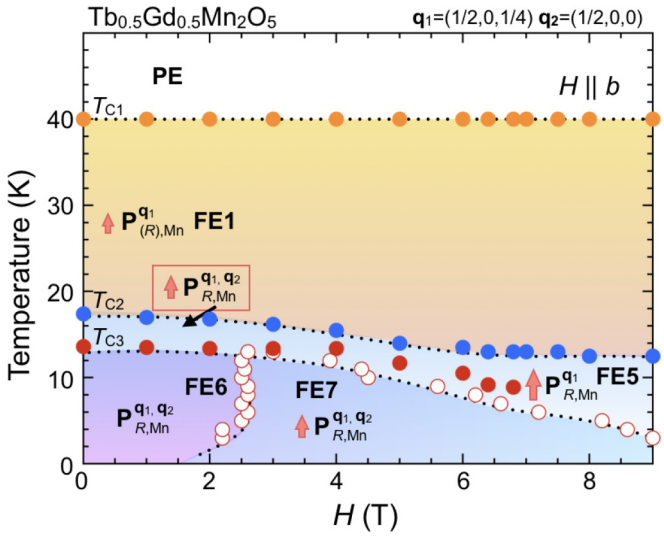

FIG. 5. Magnetoelectric phase diagram under an external magnetic field along the b axis in $Tb_{0.5}Gd_{0.5}Mn_2O_5$. Filled and open circles represent the transition temperature points obtained from dielectric measurements while increasing the temperature and magnetic-field strength, respectively. $\mathbf{P}^{\mathbf{q}_i}_{R,\mathrm{Mn}}$ corresponds to the electric polarization driven by the magnetic ordering of rare-earth and Mn ions with $\mathbf{q}_i$, where $\mathbf{q}_1 = (1/2, 0, 1/4)$ and $\mathbf{q}_2 = (1/2, 0, 0)$. The length of the red arrow represents the amplitude of the electric polarization. Magnetic orderings were observed in the present paper.

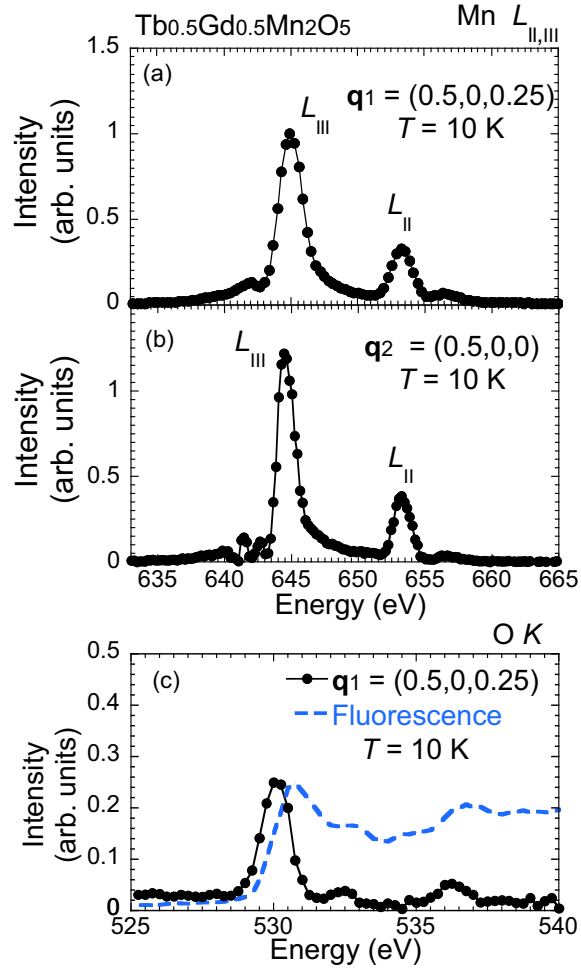

FIG. 6. Energy spectra of magnetic reflections around Mn $L_{\mathrm{II,III}}$ edges (a) at $\mathbf{q}_1 = (0.5, 0, 0.25)$, (b) at $\mathbf{q}_2 = (0.5, 0, 0)$, and (c) around the O K edge at $\mathbf{q}_1 = (0.5, 0, 0.25)$ together with the fluorescence spectrum. The fluorescence background has been subtracted from each energy spectrum.

out new potential for applications of multiferroic materials. Meanwhile the electric polarization in the FE1 phase slightly changes under magnetic field.

Magnetic-field dependence of the electric polarization and the dielectric constant at each temperature are shown in Figs. 4(g)–4(i). In these measurements, the magnetic field was applied along the b axis. Two ferroelectric phase transitions are evident at $H \sim H_1$ and $H \sim H_2$. The first transition occurs at $H \sim H_1 = 2.5$ T at each temperature and is associated with the appearance of electric polarization with a strong peak of the dielectric constant. The behavior of the dielectric constant implies that paraelectric-ferroelectric phase transition occurs at $H \sim H_1$. This ferroelectric phase is denoted as FE7. Meanwhile, the magnitude of H_2 varies with temperature. At $T = 9$ K, a second phase transition occurs at $H \sim H_2 = 6$ T, which leads to a large electric polarization. This phase appears to be equivalent to the FE5 phase based on the temperature dependence of the electric polarization and the dielectric constant shown in Figs. 4(b) and 4(e). In addition, significant magnetic-field hysteresis is also apparent at $H \sim H_2$ without obvious anomalies of the dielectric constant. This result indicates that the FE7-FE5 phase transition is a first-order transition. Figure 5 shows a magnetoelectric phase diagram under an external magnetic field along the b axis in $Tb_{0.5}Gd_{0.5}Mn_2O_5$. The transition temperature points were obtained by dielectric measurements performed while increasing temperature or magnetic-field strength. Below T_{C3}, increasing magnetic-field strength induces ferroelectric phase transition from the FE6 phase to the FE5 phase via the FE7 phase. Figure 5 also shows magnetic ordering in each phase observed in our present RXS paper (see below paragraph).

B. Resonant x-ray scattering without external magnetic field

We employed RXS to investigate the mechanism of the ME effect in $Tb_{0.5}Gd_{0.5}Mn_2O_5$. Figures 6(a) and 6(b) present the energy spectra of resonant scattering with magnetic propagation vectors $\mathbf{q}_1 = (1/2, 0, 1/4)$ and $\mathbf{q}_2 = (1/2, 0, 0)$ around Mn $L_{\mathrm{II,III}}$ edges at $T = 10$ K (in the FE6 phase) without an external magnetic field. Note that different samples were used in each of the measurements, and it is typically difficult to compare the RXS intensities acquired from different samples since the scattering intensity strongly depends on the sample surface conditions. Well-defined magnetic peaks were observed at both reciprocal lattice points, indicating that the magnetic ordering in the FE6 phase is associated with two magnetic propagation vectors $\mathbf{q}_1$ and $\mathbf{q}_2$. The temperature dependence of the intensities at the Mn L_{III} edge is shown in Fig. 7(a). Magnetic ordering with $\mathbf{q}_1$ appears at $T \sim T_{\mathrm{N1}} = 40$ K concomitant with the first ferroelectric phase transition to the FE1 phase as shown in Fig. 7(e). The resonant intensity at $\mathbf{q}_2$ increases below $T \sim T_{\mathrm{N2}} = 20$ K simultaneously with a decrease in the $\mathbf{q}_1$ intensity.

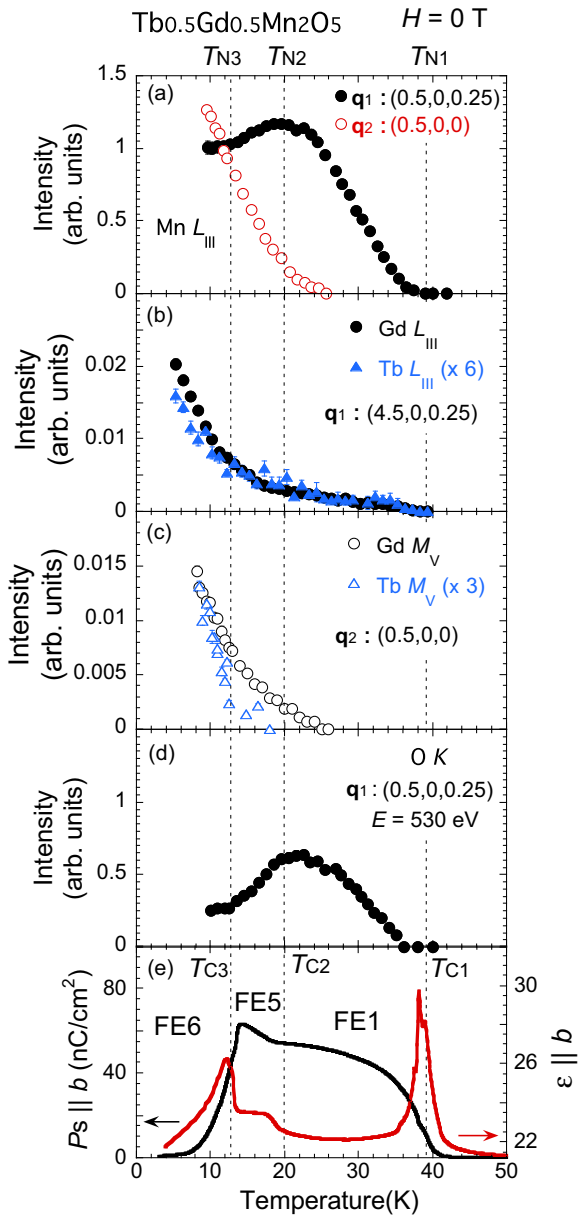

FIG. 7. Temperature dependence of resonant scattering intensity without an external magnetic field (a) at the Mn L_{III} edge at $\mathbf{q}_1 = (0.5, 0, 0.25)$ (closed circles) and at $\mathbf{q}_2 = (0.5, 0, 0)$ (open circles), (b) at Gd (closed circles) and Tb (closed triangles) L_{III} edges at (4.5, 0, 0.25), (c) at Gd (open circles), and Tb (open triangles) M_{V} edges at $\mathbf{q}_2$, and (d) at the O K edge at $\mathbf{q}_1$. (e) Temperature dependence of electric polarization (black line) and dielectric constant (red line).

Figures 7(b) and 7(c) show temperature dependence of the resonant scattering intensities with $\mathbf{q}_1$ at Gd and Tb L_{III} edges and those with $\mathbf{q}_2$ at Gd and Tb M_{V} edges, respectively. Well-defined magnetic reflections are apparent with $\mathbf{q}_1$ around Gd and Tb L_{III} edges, whereas no reflections are observed with $\mathbf{q}_2$ despite careful attempts to acquire the peaks. Meanwhile, the resonant reflections at $\mathbf{q}_1$ and $\mathbf{q}_2$ both appear at Gd and Tb M_{V} edges. This is likely due to RXS at the rare-earth M_{V} edge enabling one to detect a resonant scattering sensitively since this energy range corresponds with a direct electronic transition to $4f$ orbitals. These observations indicate that rare-earth moments also align with both $\mathbf{q}_1$ and $\mathbf{q}_2$.

The intensities at $\mathbf{q}_1$ at Gd and Tb L_{III} edges appear at $T \sim T_{\mathrm{N1}}$ and increase at $T \sim T_{\mathrm{N2}}$ and $T \sim T_{\mathrm{N3}} = 14$ K. A recent neutron-scattering study for $TbMn_2O_5$ showed a similar thermal evolution of magnitude of magnetic moments at Tb sites [17]. The intensities at $\mathbf{q}_2$ at Gd and Tb M_{V} edges appear simultaneously with that at the Mn L_{III} edge at $T \sim T_{\mathrm{N2}}$. The significant increase in both resonant intensities with $\mathbf{q}_1$ and $\mathbf{q}_2$ below T_{N3} indicates that Gd and Tb ordering with $\mathbf{q}_1$ and/or $\mathbf{q}_2$ induces the FE6 phase. Noted that the intensities at Gd and Tb M_{V} edges show slightly different thermal evolution as shown in Fig. 7(c), which might be attributed to different behavior of $\mathbf{q}_2$ magnetic ordering of Gd and Tb ions. Based on these observations, we obtained the magnetic phase diagram for $Tb_{1-x}Gd_xMn_2O_5$ provided in Fig. 1. According to this diagram, the FE1 phase is primarily associated with the Mn magnetic ordering with $\mathbf{q}_1$, whereas the FE5 phase is induced by magnetic ordering of rare-earth and Mn ions with $\mathbf{q}_1$ and/or $\mathbf{q}_2$. In the FE6 phase, a significant increase in the magnitude of magnetic moments at the rare-earth sites leads to the disappearance of the electric polarization.

We also observed spin polarization of O ions. Figure 6(c) shows energy spectrum around the O K edge at $\mathbf{q}_1$. Note that the fluorescence background has been subtracted from the resonant scattering spectrum. Similar energy spectra have been acquired from RMn_2O_5 (R = Y, Er, Tb, Gd) [22–25] and $RMnO_3$ (R = Tb, Dy)[26] compounds. Resonant peaks are observed around $E = 530$ and $E = 532.5$ eV, respectively, both of which correspond to $2p$-$3d$ hybridization between O and Mn ions [27,28]. In addition, another peak is observed around $E = 536$ eV. This energy range is associated with rare-earth $5d$ states, and similar rare-earth contributions were also observed in studies on RMn_2O_5 (R = Tb, Sm, Gd) [24,25]. These observations indicate that the spin polarization of O ions is induced by charge transfer from O to both Mn and rare-earth ions. In contrast, no magnetic signals were detected around the O K edge at $\mathbf{q}_2$ within the experimental error, although the intensities observed around the Mn $L_{\mathrm{II,III}}$ edges with $\mathbf{q}_2$ are comparable to those with $\mathbf{q}_1$ as shown in Figs. 6(a) and 6(b). Therefore the magnetic moments of O ions likely align solely with $\mathbf{q}_1$. The temperature dependence of the scattering intensity at $E = 530$ eV and at $\mathbf{q}_1$ is plotted in Fig. 7(d). Magnetic ordering with $\mathbf{q}_1$ occurs simultaneously with that of the Mn ions at $T \sim T_{\mathrm{N1}}$. At $T \sim T_{\mathrm{N2}}$, the scattering intensity is strongly suppressed compared to that at the Mn L_{III} edge.

C. Resonant x-ray scattering under external magnetic field

RXS for $Tb_{0.5}Gd_{0.5}Mn_2O_5$ was also performed under an external magnetic field, during which data were acquired while increasing the magnetic-field strength along the b axis. Figure 8(a) presents magnetic-field dependence of the resonant intensities at Mn L_{III}, Gd, and Tb M_{V} at $\mathbf{q}_1$. The intensities around Mn and Tb absorption edges are seen to slightly increase, whereas that at the Gd M_{V} edge decreases. This suggests that the external magnetic field slightly destabilizes the $\mathbf{q}_1$ ordering of Gd ions. In sharp contrast, the intensities at $\mathbf{q}_2$ dramatically decrease above $H \sim H_1$ and almost disappear at $H \sim H_2$. These data clearly demonstrate that the

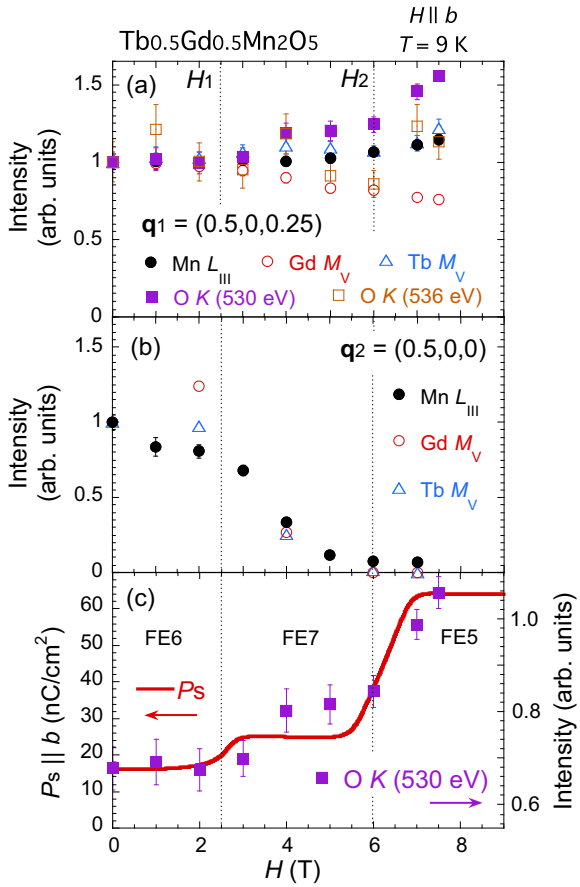

FIG. 8. Magnetic-field dependence of resonant intensity at (a) $T = 9$ K at $\mathbf{q}_1$ at Mn L_{III}, O K ($E = 530$ eV, $E = 536$ eV), Tb, and Gd M_{V} edges and (b) at $\mathbf{q}_2$ at Mn L_{III}, Tb, and Gd M_{V} edges. (c) Magnetic-field dependence of electric polarization and intensity at $E = 530$ eV. These data were obtained by increasing the external magnetic-field strength. The intensities were normalized relative to values obtained at $H = 0$ T for each data set.

disappearance of the magnetic ordering with $\mathbf{q}_2$ leads to an increase in the electric polarization. According to these measurements, we obtained the magnetoelectric phase diagram under an external magnetic field along the b axis (shown in Fig. 5). Here, magnetic ordering of Mn ions with $\mathbf{q}_1$ appears in the FE1 phase, which is not significantly affected by an external magnetic field. The electric polarization disappears in the FE6 phase in which $\mathbf{q}_1$ and $\mathbf{q}_2$ magnetic ordering of Mn and rare-earth ions coexist. The application of an external magnetic field decays the magnetic ordering with $\mathbf{q}_2$, which, in turn, causes ferroelectric phase transitions from FE6 to FE5 via FE7, resulting in the ME effect. Conversely, in the FE5 phase, disappearance of the magnetic ordering with $\mathbf{q}_2$ appears to have little effect on the electric polarization. This finding suggests that $\mathbf{q}_2$ ordering makes only a minor contribution to the FE5 phase.

As shown in Figs. 4(a)–4(c), $Tb_{0.5}Gd_{0.5}Mn_2O_5$ exhibit a colossal ME effect in response to the magnetic field applied along any of the crystallographic axes. This isotropic ME effect implies that the Gd^{3+} ions, which are isotropic due to their zero orbital angular momentum $\mathbf{L} = 0$, play a key role. Previous RXS and neutron-scattering experiments for $GdMn_2O_5$ have indicated that magnetic ordering of the Gd ions preferentially induces the $\mathbf{q}_2$ magnetic ordering [9,10]. Hence, it is probable that modulation of the Gd magnetic ordering induced by an external magnetic field results in the decay of the $\mathbf{q}_2$ magnetic ordering of all ions, which leads to the isotropic ME effects. Meanwhile, $Tb_{0.5}Gd_{0.5}Mn_2O_5$ exhibits slight anisotropy in the ME effect, which is likely due to the single-ion anisotropy of Tb^{3+} ions. Further understanding of the mechanism of this ME effect would require clarification of the magnetic structure of the material, and we intend to perform neutron scattering for $Tb_{0.5}Gd_{0.5}Mn_2O_5$ using isotope Gd ions in the future.

Figure 8(a) also shows the magnetic-field dependence of the resonant intensities at $E = 530$ and $E = 536$ eV around the O K edge. The intensity at $E = 530$ eV increases to a greater extent than those at other element absorption edges, whereas that at $E = 536$ eV does not show any significant changes. Figure 8(c) again shows magnetic-field dependence of the electric polarization and the intensity at $E = 530$ eV. Remarkably, both of them exhibit almost the same magnetic-field dependence. A recent RXS study of YMn_2O_5 suggested that spin polarization at O sites reflects the magnetically driven charge transfer between O and Mn ions, which plays a major microscopic role in the electric polarization [23]. Our observations as reported herein suggest that this charge transfer makes the primary microscopic contribution to the ME effect in $Tb_{0.5}Gd_{0.5}Mn_2O_5$. The data also imply that charge transfer is the common origin for the ME effects exhibited by the members of the RMn_2O_5 family and by other multiferroic compounds. Further theoretical and experimental studies are required for a greater understanding of local mechanism of the ME effects.

IV. SUMMARY

An isotropic ME effect is discovered in $Tb_{1-x}Gd_xMn_2O_5$. In particular, the electric polarization of $Tb_{0.5}Gd_{0.5}Mn_2O_5$ disappears when it transitions to the FE6 phase and reappears in response to an external magnetic field applied along each crystallographic axis. This isotropic ME effect is quite unique among the members of the RMn_2O_5 family and among other multiferroic compounds. Our RXS study indicated that the appearance of the rare-earth magnetic ordering with $\mathbf{q}_1$ and $\mathbf{q}_2$ leads to the disappearance of the electric polarization in the FE6 phase and that a decay of the magnetic ordering with $\mathbf{q}_2$ in response to an external magnetic field results in the reappearance of the electric polarization. In addition, the magnetic-field dependence of spin polarization at O sites suggests that the charge transfer between O and Mn ions microscopically contributes to the ME effect in this material.

ACKNOWLEDGMENTS

This study was supported by the KAKENHI Program for Scientific Research (A) (Programs No. JP15H02038, No. JP15H05885(J-Physics), No. JP17K05130), (B) (No. 24340064), and Young Scientists (B) (No. 16K17759), Challenging Exploratory Research (Grant No. 2365409), Dynamic Alliance for Open Innovation Bridging Human, Environment

and Materials, and Condensed Matter Research Center (CMRC) in KEK. This work was performed with the approval of the Photon Factory Program Advisory Committee (Proposals No. 2016PF-BL-19B, No. 2017G018, and No. 2017G549).

[1] T. Kimura, T. Goto, H. Shintani, K. Ishizaka, T. Arima, and Y. Tokura, Nature (London) **426**, 55 (2003).
[2] K. Taniguchi, N. Abe, T. Takenobu, Y. Iwasa, and T. Arima, Phys. Rev. Lett. **97**, 097203 (2006).
[3] N. Hur, S. Park, P. A. Sharma, J. S. Ahn, S. Guha, and S.-W. Cheong, Nature (London) **429**, 392 (2004).
[4] M. Fukunaga, Y. Sakamoto, H. Kimura, Y. Noda, N. Abe, K. Taniguchi, T. Arima, S. Wakimoto, M. Takeda, K. Kakurai, and K. Kohn, Phys. Rev. Lett. **103**, 077204 (2009).
[5] H. Kimura, S. Wakimoto, M. Fukunaga, Y. Noda, K. Kaneko, N. Metoki, K. Kakurai, and K. Kohn, J. Phys. Soc. Jpn. **78**, 034718 (2009).
[6] H. Kimura, S. Kobayashi, Y. Fukuda, T. Osawa, Y. Kamada, Y. Noda, I. Kagomiya, and K. Kohn, J. Phys. Soc. Jpn. **76**, 074706 (2007).
[7] Y. Noda, H. Kimura, M. Fukunaga, S. Kobayashi, I. Kagomiya, and K. Kohn, J. Phys.: Condens. Matter **20**, 434206 (2008).
[8] C. Vecchini, L. C. Chapon, P. J. Brown, T. Chatterji, S. Park, S-W. Cheong, and P. G. Radaelli, Phys. Rev. B **77**, 134434 (2008).
[9] N. Lee, C. Vecchini, Y. J. Choi, L. C. Chapon, A. Bombardi, P. G. Radaelli, and S.-W. Cheong, Phys. Rev. Lett. **110**, 137203 (2013).
[10] G. Yahia, F. Damay, S. Chattopadhyay, V. Balédent, W. Peng, S. W. Kim, M. Greenblatt, M.-B. Lepetit, and P. Foury-Leylekian, Phys. Rev. B **97**, 085128 (2018).
[11] Y. Ishii, S. Horio, M. Mitarashi, T. Sakakura, M. Fukunaga, Y. Noda, T. Honda, H. Nakao, Y. Murakami, and H. Kimura, Phys. Rev. B **93**, 064415 (2016).
[12] G. Yahia, F. Damay, S. Chattopadhyay, V. Balédent, W. Peng, E. Elkaim, M. Whitaker, M. Greenblatt, M.-B. Lepetit, and P. Foury-Leylekian, Phys. Rev. B **95**, 184112 (2017).
[13] L. C. Chapon, P. G. Radaelli, G. R. Blake, S. Park, and S.-W. Cheong, Phys. Rev. Lett. **96**, 097601 (2006).
[14] J.-H. Kim, S.-H. Lee, S. I. Park, M. Kenzelmann, A. B. Harris, J. Schefer, J.-H. Chung, C. F. Majkrzak, M. Takeda, S. Wakimoto, S. Y. Park, S-W. Cheong, M. Matsuda, H. Kimura, Y. Noda, and K. Kakurai, Phys. Rev. B **78**, 245115 (2008).
[15] S. Wakimoto, H. Kimura, Y. Sakamoto, M. Fukunaga, Y. Noda, M. Takeda, and K. Kakurai, Phys. Rev. B **88**, 140403(R) (2013).
[16] S. Kobayashi, T. Osawa, H. Kimura, Y. Noda, N. Kasahara, S. Mitsuda, and K. Kohn, J. Phys. Soc. Jpn. **73**, 3439 (2004).
[17] C. Wilkinson, P. J. Brown, and T. Chatterji, Phys. Rev. B **84**, 224422 (2011).
[18] S. H. Bukhari, Th. Kain, M. Schiebl, A. Shuvaev, A. Pimenov, A. M. Kuzmenko, X. Wang, S.-W. Cheong, J. Ahmad, and A. Pimenov, Phys. Rev. B **94**, 174446 (2016).
[19] B. M. Wankly, J. Mater. Sci. **7**, 813 (1972).
[20] H. Nakao, Y. Yamasaki, J. Okamoto, T. Sudayama, Y. Takahashi, K. Kobayashi, R. Kumai, and Y. Murakami, J. Phys.: Conf. Ser. **502**, 012015 (2014).
[21] J. Okamoto, H. Nakao, Y. Yamasaki, T. Sudayama, K. Kobayashi, Y. Takahashi, H. Yamada, A. Sawa, M. Kubota, R. Kumai, and Y. Murakami, J. Phys.: Conf. Ser. **502**, 012016 (2014).
[22] R. A. de Souza, U. Staub, V. Scagnoli, M. Garganourakis, Y. Bodenthin, S.-W. Huang, M. García-Fernández, S. Ji, S.-H. Lee, S. Park, and S.-W. Cheong, Phys. Rev. B **84**, 104416 (2011).
[23] S. Partzsch, S. B. Wilkins, J. P. Hill, E. Schierle, E. Weschke, D. Souptel, B. Büchner, and J. Geck, Phys. Rev. Lett. **107**, 057201 (2011).
[24] T. A. W. Beale, S. B. Wilkins, R. D. Johonson, D. Prabhakaran, A. T. Boothroyd, P. Steadman, S. S. Dhesi, and P. D. Hatton, Eur. Phys. J. Spec. Top. **208**, 99 (2012).
[25] Y. Ishii, S. Horio, H. Yamamoto, Y. Noda, H. Nakao, Y. Murakami, and H. Kimura, Phys. Rev. B **98**, 174428 (2018).
[26] S. W. Huang, J. M. Lee, H.-T. Jeng, Y.C. Shao, L. A. Wray, J. M. Chen, R. Qiao, W. L. Yang, Y. Cao, J.-Y. Lin, R. W. Schoenlein, and Y.-D. Chuang, Phys. Rev. B **94**, 035145 (2016).
[27] F. El Hallani, S. Naji, H. Ez-Zahraouy, and A. Benyoussef, J. Appl. Phys. **114**, 163909 (2013).
[28] M. Ait Tamerd, B. Abraime, A. Abbassi, K. El Maalam, A. El Kenz, A. Benyoussef, M. Balli, M. Hamedoun, and O. Mounkachi, J. Phys: Conf. Ser. **758**, 012009 (2016).